4.4.3 Uncorrelated Transverse Momentum

We now turn to the case of transverse momentum. We have seen that traditional electron spectroscopy techniques allow for the determination of the longitudinal momentum transfer (P_z) to each of the three participants in the collision [2.2]. In this case however, because no measurement of the momentum of either the recoil-ion or projectile is made, complete measurements of the transverse momentum exchanges are not possible. Let us restate this specifically. In addition to $d\sigma/dp_{e//}$ and $d\sigma/dp_{R//}$, we are able to measure $d\sigma/d\mathbf{p}_{e\perp}$ and $d\sigma/d\mathbf{p}_{R\perp}$, and these measurements in coincidence allow us to infer $d\sigma/d\mathbf{p}_{P\perp}$. With traditional electron spectroscopy, one can measure $d\sigma/d\mathbf{p}_e$ and infer $d\sigma/dp_{R//}$ and $d\sigma/dp_{P//}$, but not $d\sigma/d\mathbf{p}_{P\perp}$ and $d\sigma/d\mathbf{p}_{R\perp}$ separately.

One of the simplest presentations of our data is the uncorrelated momentum distributions for the electrons and recoil ions. These are the quantites that we measure directly, and even without taking into account the coincident nature of our experiment, we are able to gain some insight into the general behavior the participants in these collisions. To remind the reader of the apparatus geometry, the x- and y-axes are perpendicular to the beam (z-) axis and defined by the directions of the electric field and the gas jet respectively. The transverse momentum distributions of the electrons and recoil ions should be cylindrically symmetric about the z-axis. The transverse recoil momentum for each of three collision systems is shown in Figure 4.12. The rectangles represent the calculated momentum resolution for each case.

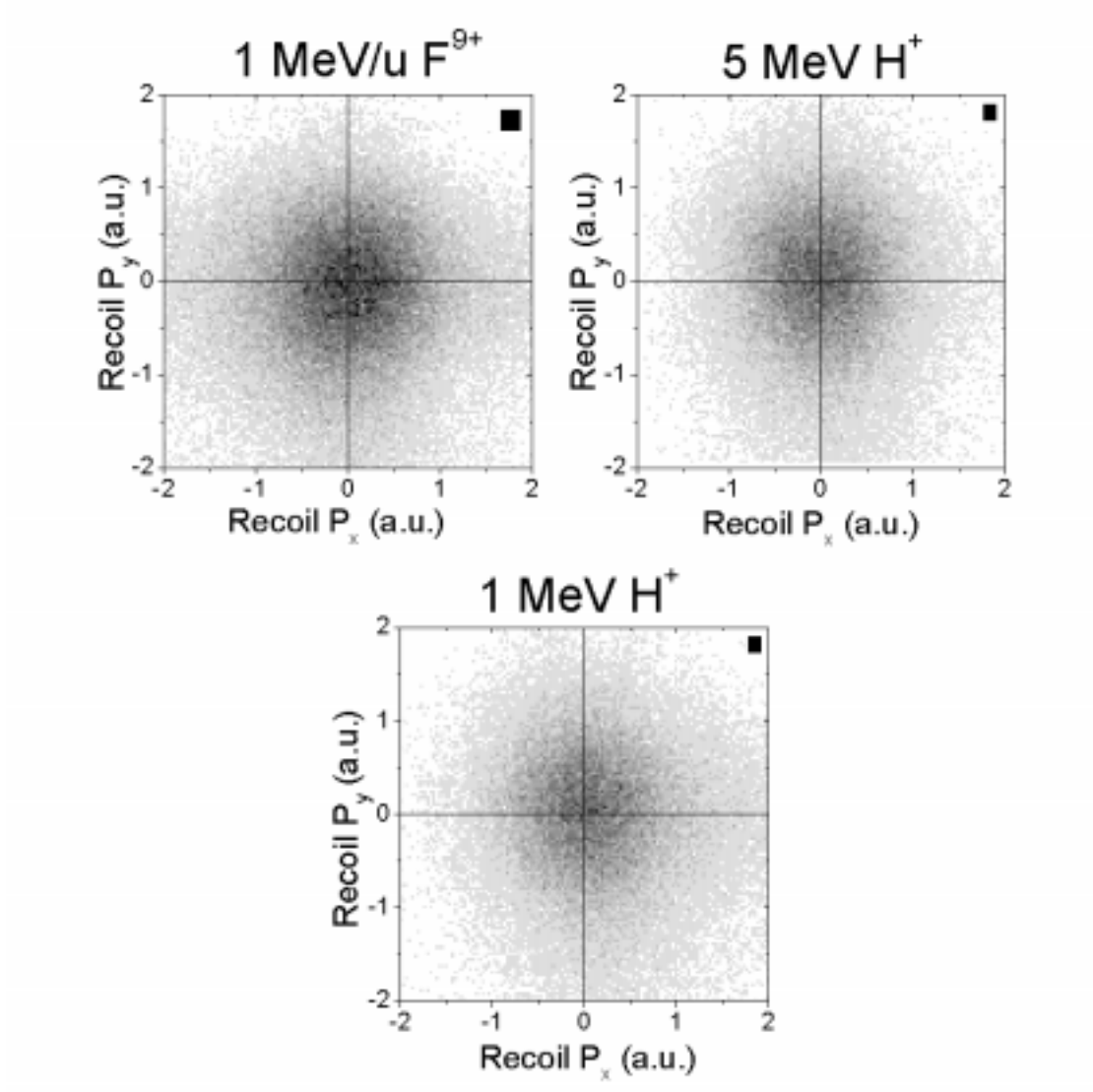

Figure 4.12: Density plots of the doubly differential cross sections $d^2\sigma/dP_{xR}\,dP_{yR}$ (transverse recoil momentum) for the three collision systems. The black rectangles represent the resolution in either direction.

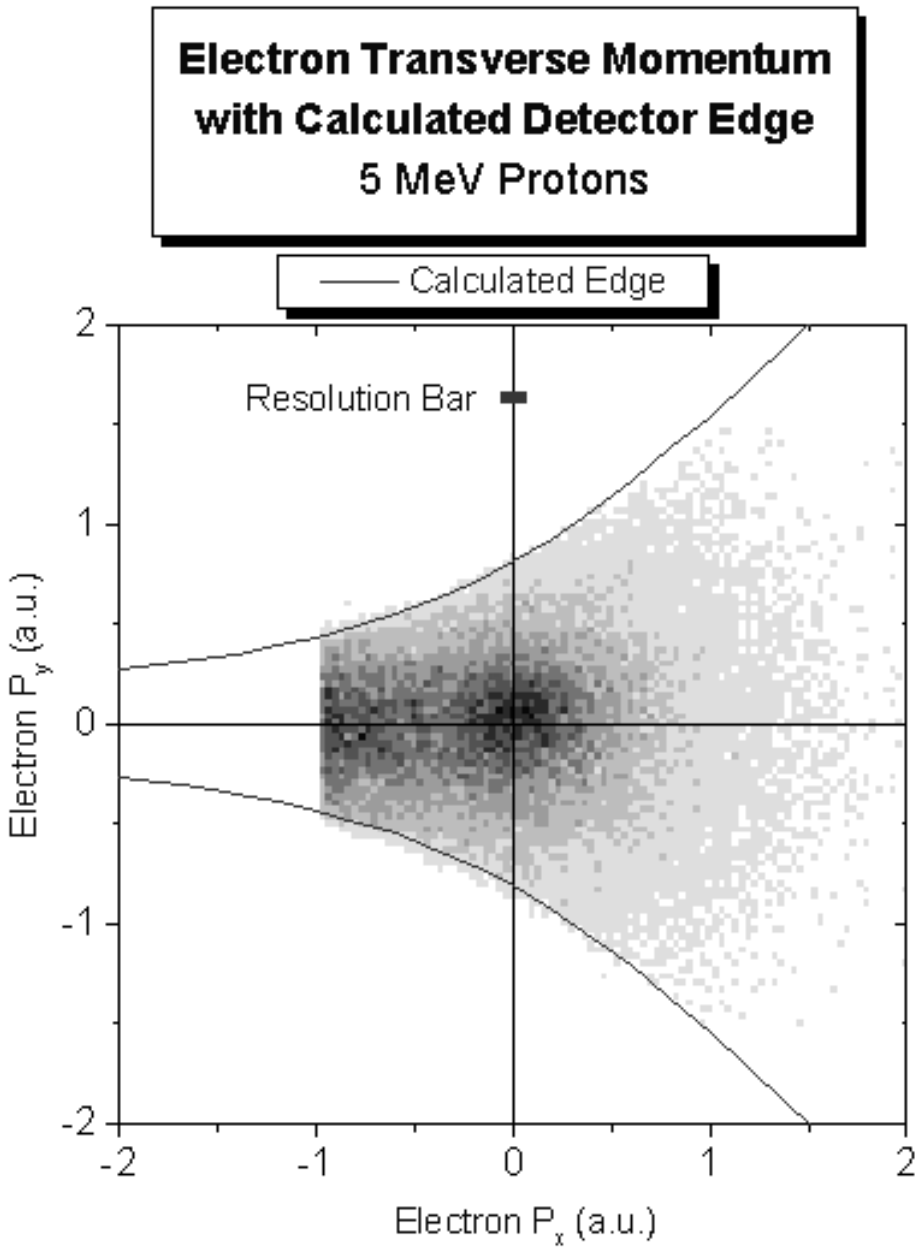

Figure 4.13: Density plots of the doubly differential cross section $d^2\sigma / dP_{xe}\, dP_{ye}$ (transverse electron momentum) for collision system 5 MeV H^+ + He. The black rectangles represent the resolution in either direction. The curved lines represent the simulated detector edge in momentum space.

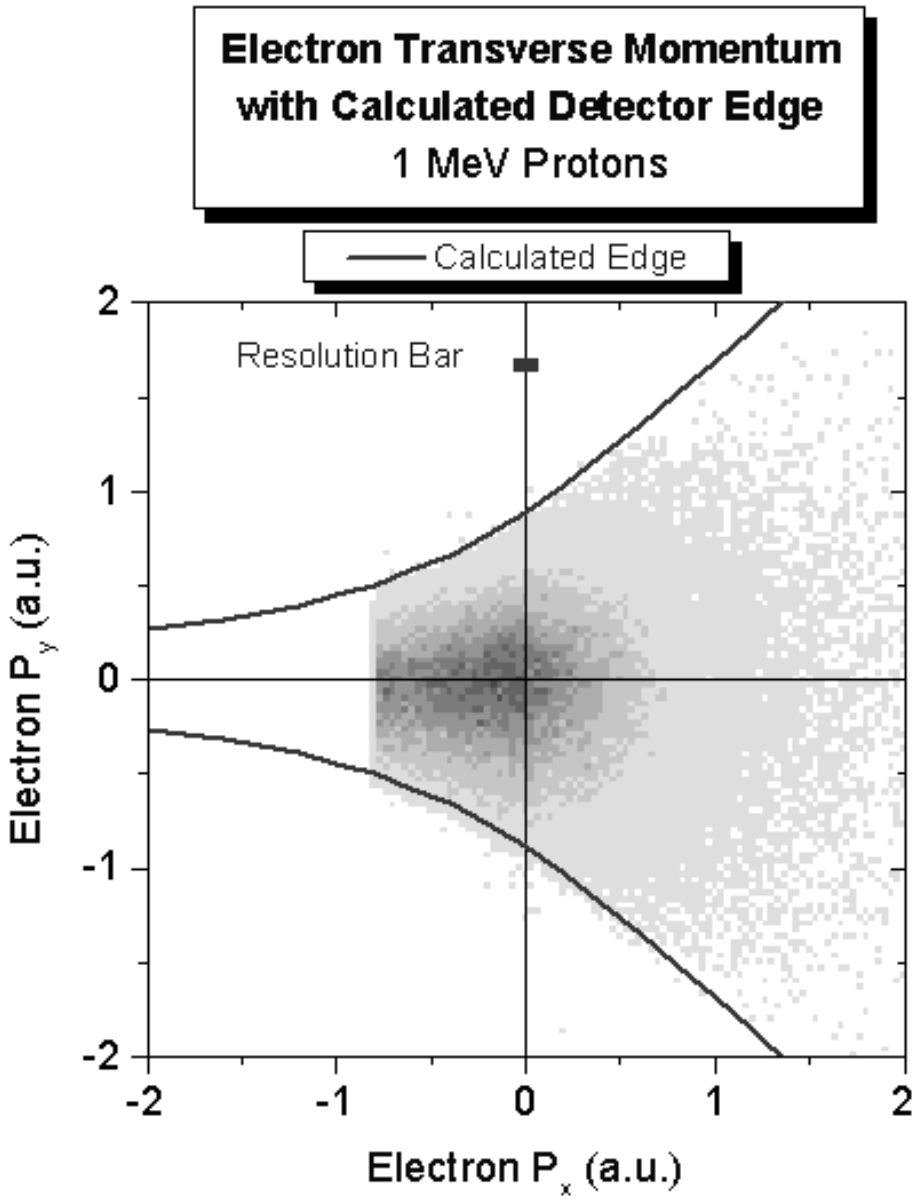

Figure 4.14: Density plots of the doubly differential cross section $d^2\sigma / dP_{xe}\, dP_{ye}$ (transverse electron momentum) for collision system 1 MeV H^+ + He. The black rectangles represent the resolution in either direction. The curved lines represent the simulated detector edge in momentum space.

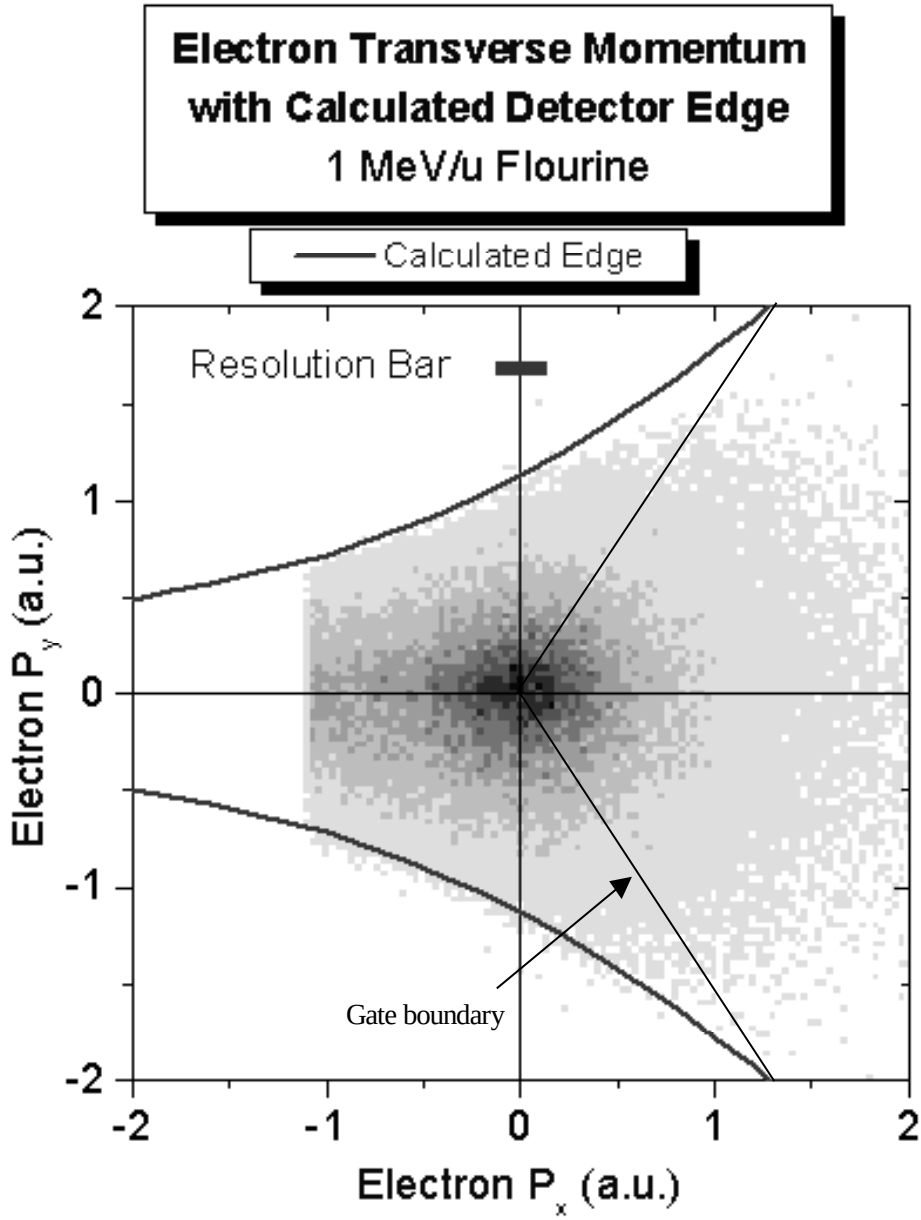

Figure 4.15: Density plots of the doubly differential cross section $d^2\sigma / dP_{xe}\, dP_{ye}$ (transverse electron momentum) for collision system 1 MeV/amu F^{9+} + He. The black rectangles represent the resolution in either direction. The curved lines represent the simulated detector edge in momentum space. The straight diagonal lines define the boundaries of the momentum gate.

The resolution in the case of the fluorine beam is larger due to the higher field required. The x- and y- momenta were calibrated independently of one another. The distributions are cylindrically symmetric, with a slight tail toward the negative y-direction due to the hot gas. They are all plotted on the same scale for comparison.

Similar spectra for the electrons are shown in figures 4.13-4.15. In the electron case, the time of flight played a much more critical role in not only determining the x-momentum, but the y- and z- cases as well. In fact, as can be seen in the figures, only electrons of particular coordinates in momentum space made it onto the detector. This is analogous to throwing a baseball. Throwing the ball partially upward allows one to throw it farther; in the same way, electrons with momentum partially away from the detector traveled beyond its edge. The same simulation used to convert from electron TOF to P_x was also used to predict the detector edge in momentum space (Appendix A). The data fell within these boundaries almost exactly. The only observable deviation is accounted for by the beam not passing directly in front of the center of the detector. Due to this edge effect, the solid angle toward and away from the detector varied dramatically with energy. Therefore, to avoid bias for lower energy electrons not truncated by this effect, we required the data to fall within a gate placed on the 2-d transverse electron spectrum. An example of this gate may be seen in figure 4.15, noted with the label "gate boundary." Only events to the right of this boundary were accepted in the final analysis.

Figure 4.16 shows the 1-d distributions of electron and recoil transvere

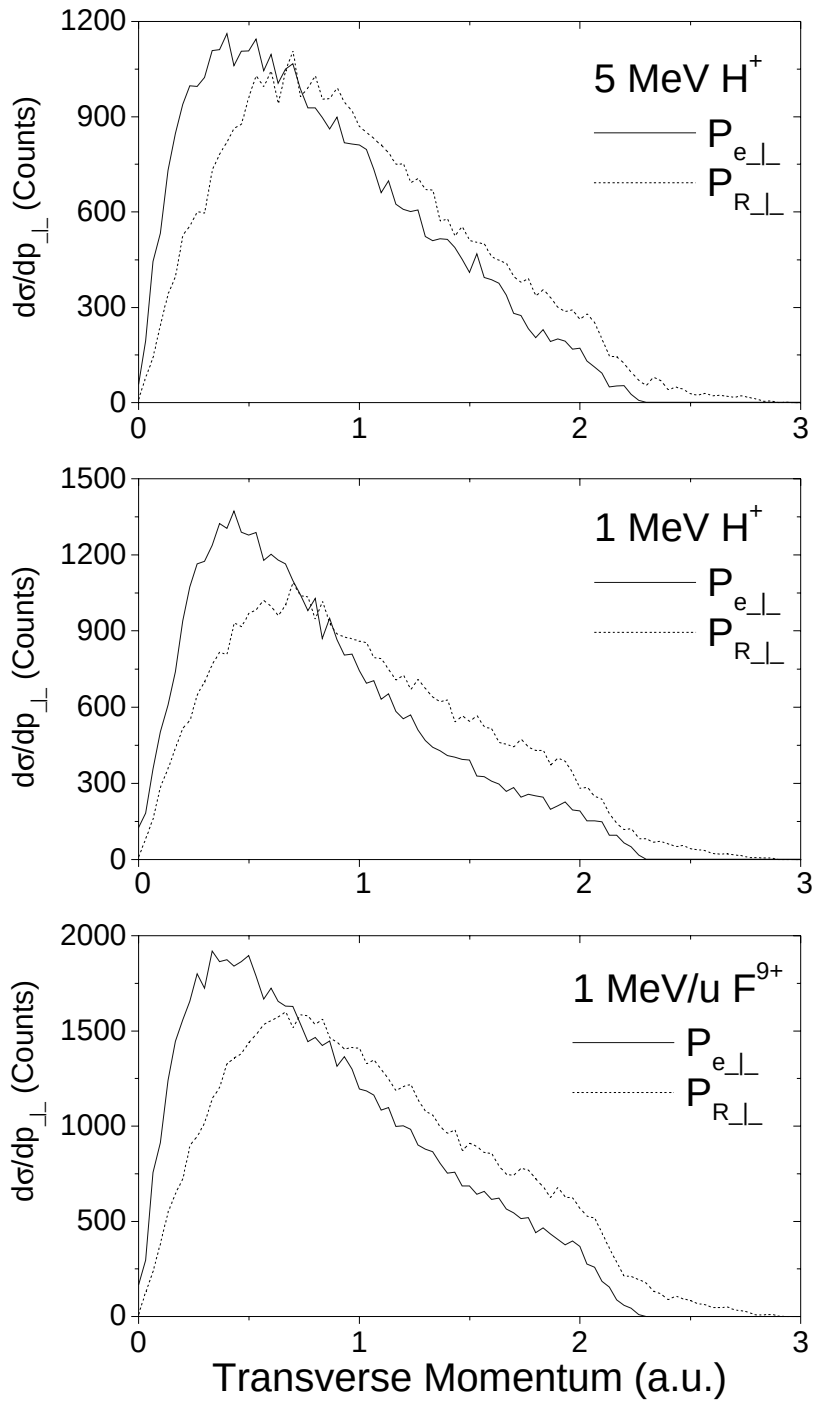

Figure 4.16: Radial distributions of transverse electron and recoil momenta.

momentum for all three collision systems. The recoil ion distribution for each system is substantially broader than that of the electrons. This imbalance must be reconciled by the projectile's transverse momentum, implying the presence of a nuclear or binary encounter type scattering.

4.4.4 Correlated Transverse Momentum

In order to discern the interrelationships between the three vectors in the transverse plane, it is most useful to study the correlation between one vector and another. Once again, as a reminder, the electron and recoil momentum vectors are measured, while the projectile vector is inferred by conservation of transverse momentum. We will begin with figures 4.16-4.18. In the same manner as in the longitudinal case, we have plotted the recoil P_x (or P_y) versus the electron P_x (or P_y), all of which are directly measured quantities. The data for low electron P_x were contaminated by the aforementioned echoes in the TAC peak and were omitted for quality control. If the scattering were photoionization-like, there would be a complete momentum balance between the electron and recoil, causing the data in these figures to lie along a line with slope of –1. This is not the case for any of